PHYSICAL REVIEW D **96,** 104033 (2017)

New method for enhanced efficiency in detection of gravitational waves from supernovae using coherent network of detectors

S. Mukherjee,[*] L. Salazar,[†] J. Mittelstaedt,[‡] and O. Valdez

Center for Gravitational Wave Astronomy, Department of Physics, The University of Texas Rio Grande Valley, One West University Boulevard, Brownsville, Texas 78520, USA

(Received 22 December 2016; published 20 November 2017)

Supernovae in our universe are potential sources of gravitational waves (GW) that could be detected in a network of GW detectors like LIGO and Virgo. Core-collapse supernovae are rare, but the associated gravitational radiation is likely to carry profuse information about the underlying processes driving the supernovae. Calculations based on analytic models predict GW energies within the detection range of the Advanced LIGO detectors, out to tens of Mpc for certain types of signals e.g. coalescing binary neutron stars. For supernovae however, the corresponding distances are much less. Thus, methods that can improve the sensitivity of searches for GW signals from supernovae are desirable, especially in the advanced detector era. Several methods have been proposed based on various likelihood-based regulators that work on data from a network of detectors to detect burst-like signals (as is the case for signals from supernovae) from potential GW sources. To address this problem, we have developed an analysis pipeline based on a method of noise reduction known as the harmonic regeneration noise reduction (HRNR) algorithm. To demonstrate the method, sixteen supernova waveforms from the Murphy *et al.* 2009 catalog have been used in presence of LIGO science data. A comparative analysis is presented to show detection statistics for a standard network analysis as commonly used in GW pipelines and the same by implementing the new method in conjunction with the network. The result shows significant improvement in detection statistics.

DOI: 10.1103/PhysRevD.96.104033

I. INTRODUCTION

Supernovae (SN) in our universe are potential sources of gravitational waves (GW) [1–3] that could be detected in a network of GW detectors. Several GW detectors are in operation, e.g., like LIGO [4], Virgo [5], and GEO600 [6]. Core-collapse supernovae are rare, but the associated gravitational radiation is likely to carry profuse information about the underlying processes driving the supernovae. Calculations based on analytic models predict GW energies within the detection range of the Advanced LIGO [7] detectors, out to tens of kpc.

Analysis of the GW signal of the post-bounce evolution of core-collapse supernovae using relativistic, two-dimensional explosion models have been calculated [8]. The waveforms show the accelerated mass motions associated with the characteristic evolutionary stages, which were also seen in previous studies [9,10]. The basic model is that a quasi-periodic modulation by prompt post-shock convection is followed by a phase of relative quiescence. Following this, the amplitudes grow again due to violent hydrodynamical activity caused by convection and the standing accretion shock instability. Finally, a high-frequency, low-amplitude variation from proto-neutron star convection below the neutrinosphere appears superimposed on the low-frequency trend associated with the aspherical expansion of the SN shock after the onset of the explosion. The GW frequency from neutrino driven core collapse supernovae is expected to evolve from approximately100 Hz to about 1000 Hz.

Since the signals from these sources are weak, methods that can improve the sensitivity of searches for GW signals from SN are desirable, especially in the advanced detector era. Several methods have been proposed [11–13] based on various likelihood-based regulators that work on data from a network of detectors to detect burst-like signals (as is the case for signals from supernovae) from potential GW sources. To address this problem, we have developed and implemented a new technique of noise reduction in the supernova search pipeline based on harmonic regeneration noise reduction (HRNR) algorithm [14–17]. The method is based on a multi-stage, high accuracy spectral estimation to effectively achieve higher signal to noise ratio (snr).

The paper is organized as follows. Section II to V describes the algorithm development in detail. Section VI describes the analysis pipeline where sixteen supernova waveforms from the Murphy *et al.* 2009 catalog [9] have been used in presence of LIGO science data. A comparative analysis is presented to show detection statistics for a standard network analysis as commonly used in GW pipelines and the same by implementing the new method in conjunction with the network. Section VII discusses the results and Sec. VIII summarizes the conclusion.

[*]Corresponding author.
soma.mukherjee@utrgv.edu
[†]Information Technology Department, University of Texas Rio Grande Valley.
[‡]Permanent address: Department of Physics, University of Chicago, 5720 S. Ellis Avenue, Chicago, IL 60637, USA.

II. REVIEW OF PREVIOUS STUDY

Logue *et al.* [18] have used the supernova model extraction extractor (SMEE) algorithm to infer physical information from core-collapse supernovae. SMEE is a Bayesian approach where simulated supernovae signals are decomposed into principal components and a nested sampling algorithm [19,20] to classify the injected signal as to belonging to a particular model in given supernovae catalogs [21]. The study uses simulated Advanced LIGO noise and a single detector to demonstrate that the method successfully distinguishes magnetorotational explosions in the Milky Way galaxy (distance ≤ 10 kpc) and the neutrino driven explosions (distance ≤ 2 kpc). Moreover, the method is able to accurately differentiate between rotating accretion-induced model for white dwarves and rotating iron core-collapse up to several kpc. While the study is one of the first systematic attempt to infer core-collapse physics from the SMEE detection and classification algorithm, it uses some simplifying assumptions e.g. Gaussian noise, linear polarization and optimally oriented GW emission.

Gossan *et al.* [22] have discussed detection of GW from CCSN using a network of detectors. The method used is called the X-Pipeline [23], a coherent network analysis pipeline that searches for excess power in time-frequency space. The study shows that neutrino-driven CCSN can be detected up to 5.5 kpc, while rapidly rotating CCSN can be detected all the way up to 50 kpc (Large Magellanic Cloud.) Extreme GW emission models [24,25] are detectable out to 0.77 Mpc.

In a 2016 study, Powell *et al.* [26] demonstrated for the first time that SMEE can determine explosion mechanism up to galactic distances in presence of real non-Gaussian and nonstationary noise. The authors inferred that GW signals from neutrino-driven convection have a smaller amplitude than those from rapidly-rotating core collapse. Model selection is enhanced by a careful selection of the number of principal components that considers the relative complexity of the dierent explosion models.

Hayama *et al.* [27] have studied three dimensional hydrodynamical simulation models for detection, reconstruction, and source localization of the gravitational-wave (GW) signals using a coherent network of detectors (RIDGE pipeline) that included the network of LIGO Hanford, LIGO Livingston, VIRGO and Kagra [28]. The output of their pipeline could recover several important hydrodynamics features in the original waveforms. The authors identified the excess in the spectrograms to the features of the collapse process. Not only were the rotating core collapse, bounce, and subsequent ringdown of the proto-neutron star seen, but also formation of magnetohydrodynamics jets and nonaxisymmetric instabilities in the vicinity of the proto-neutron star could be recognized. The horizon distance was up to 18 kpc for the most rapidly rotating 3D model in this work. Following the rotating core bounce, the dominant source of the GW emission shifts to the nonaxisymmetric instabilities. The horizon distances extended up to 40 kpc when seen from the spin axis.

III. METHOD

Noise reduction can be viewed as an estimation problem, where an unknown signal is to be estimated in the presence of noise, where only the noisy observation is available. We achieve noise reduction by exploiting the spectral diversity between the signal and the noise, along with the high degree of the nonstationarity of the signal. Consequently, it is natural to perform enhancement in the frequency domain. We closely follow the development in [14]. The method comprises replacing the input data to the pipeline with the noise-reduced data.

We assume that the data segments used in the analysis satisfy assumptions of wide-sense stationarity (WSS) [29,30].

Let us first establish some basic definitions.

In general, a WSS process $x(t)$ is a weak form of stationary process in which the first and the second moments don't vary significantly with respect to time. In other words the mean is constant, i.e.

$$E[x(t)] = E(x(t+\tau)), \quad \forall\ \tau. \tag{1}$$

Here $E[x(t)]$ denotes the expectation value.

The correlation function depends only on the difference between two time instances, i.e.

$$\begin{aligned} E[x(t_1)x(t_2)] &= E(t_1, t_2) = E(t_1+\tau, t_2+\tau) \\ &= E(t_1 - t_2, 0), \quad \forall\ \tau, t_1, t_2 \end{aligned} \tag{2}$$

We will now write the discrete Fourier transform (DFT) coefficients as $X(p,k)$. Thus, $|X(p,k)|$ is the amplitude spectrum. Here, k is the frequency bin index and p is the time frame (or segment) index. The variance of the signal's DFT coefficients is given by $\sigma^2_{XX}(p,k) = E(|X(p,k)|^2)$. The periodogram is defined as $\frac{1}{K}|X(p,k)|^2$, where K is the length of each time frame. The power spectral density (psd) is defined as $P_{XX}(p,k) = \frac{1}{K}E(|X(p,k)|^2)$, for $K \to \infty$.

The basic problem can be stated as follows. We assume an additive noise model.

$$x_p(t) = s_p(t) + n_p(t) \tag{3}$$

where $x(t)$ is the data stream, $s(t)$ is the signal, embedded in noise $n(t)$. Here t denotes the discrete time index of the segment p.

Because of the linearity of the fourier transform, the noise model is expressed in the frequency domain as

$$X(p,k) = S(p,k) + N(p,k). \tag{4}$$

Here $X(p,k)$, $S(p,k)$ and $N(p,k)$ are DFT coefficients obtained at frequency index k and time frame p for noisy

data, signal and noise respectively. It is reasonable to assume that S and N are independent. Therefore, the correlation between them is zero, i.e.

$$E[S(p,k)N(p,k)] = 0, \quad \forall\ k,p. \tag{5}$$

Thus, the relation between the corresponding psd's is given by

$$P_{XX}(p,k) = P_{SS}(p,k) + P_{NN}(p,k). \tag{6}$$

Our aim is to find an estimator $\tilde{S}(p,k)$ of the signal from the noisy observed data $X(p,k)$ such that expectation value of distortion between the true signal and its estimate based on spectral noisy features is minimized. In other words, the estimate $\tilde{S}(p,k)$ of the signal is a function (denoted by $\mathcal{F}$) of all three quantities—signal psd, noise psd and the observed data,

$$\hat{S}(p,k) = \mathcal{F}(P_{NN}(p,k), P_{SS}(p,k), x(p,k)). \tag{7}$$

This is further developed in more explicit details later in this section through Eqs. (12)–(15).

Since we do not have a unique spectral estimate (the noise floor being nonstationary), we begin by estimating the snr from the noisy data.

An estimate of $S(p,k)$ is then obtained by applying a spectral gain $\Gamma(p,k)$ to each short-time spectral component $X(p,k)$.

The most widely accepted definition of the snr [31] in the GW literature is given by

$$snr = \left[4\int_0^\infty df \frac{|\tilde{s}(f)|^2}{(N(f))}\right]^{\frac{1}{2}}. \tag{8}$$

Here, $N(f)$ is the one-sided psd of the noise and $\tilde{s}(f)$ is the fourier transform of GW time domain data $s(t)$.

In keeping with the general definition of the snr, which is the ratio of the signal power to the noise power, at this point, for convenience in further derivation, two parameters are introduced: the *a posteriori* snr and the *a priori snr*, *respectively defined by*

$$snr_{\text{post}}(p,k) = \frac{|X(p,k)|^2}{P_{NN}(p,k)} \tag{9}$$

and

$$snr_{\text{priori}}(p,k) = \frac{P_{SS}(p,k)}{P_{NN}(p,k)}. \tag{10}$$

We also define the instantaneous *snr as follows.*

$$snr_{ins}(p,k) = \frac{|X(p,k)|^2 - P_{NN}(p,k)}{P_{NN}(p,k)} = snr_{\text{post}}(p,k) - 1. \tag{11}$$

$snr_{ins}(p,k)$ is taken as a measured estimate of the local *a priori* snr in a spectral subtraction approach [32]. We would like to note that the *a priori* and *a posteriori* are not used in a Bayesian sense, but rather to denote the previous and subsequent data segments in the analysis.

In reality, $P_{NN}(p,k)$ and $P_{SS}(p,k)$ are both unknown and need to be estimated. $P_{NN}(p,k)$ can be estimated by the classical minimum statistics methods [15,33]. This method provides a good estimate of psd even in presence of nonstationarity of noise. The method involves tracking spectral minima in each frequency band and minimization of a mean square estimation error (MMSE) in each time step. Specifically, if we describe $\chi_1,\chi_2,\chi_3,\ldots,\chi_n$ as the minima in the frequency bands, we can make an estimate of $P_{NN}(p,k)$ in the following way. Let $P'_{NN}(p,k)$ represent such an estimator of $P_{NN}(p,k)$. The error in the above estimate is

$$\varepsilon(\mathbf{X}) = P_{NN}(p,k) - P'_{NN}(p,k). \tag{12}$$

Since ε is a random variable, $E\{|\varepsilon|^2\}$ represents the mean square error. Under the MMSE, the best estimator for $P_{NN}(p,k)$ is given by the conditional mean

$$P'_{NN}(p,k) = E[P_{NN}(p,k)|\boldsymbol{\chi}]. \tag{13}$$

This leads to an optimal unbiased smoothed estimate of the spectral density.

After this, the spectral gain is expressed as follows.

$$\Gamma(p,k) = f(\widehat{snr}_{\text{priori}}(p,k), \widehat{snr}_{\text{post}}(p,k)). \tag{14}$$

The function f is chosen in this case to be a Wiener filter [34] described below. The signal estimate can then be obtained as follows.

$$\hat{S}(p,k) = \Gamma(p,k)X(p,k) \tag{15}$$

A. Wiener filter

The Wiener filter is based on the MMSE between the estimated signal and the true signal. The basic assumption here is that the s_p and n_p are jointly WSS with known covariance functions $R_s(p)$, $R_n(p)$ and $R_{sn}(p)$. The aim of the process is to estimate s_p as a function of x by finding the linear MMSE estimate of s_p based on x_p.

Let us consider a finite impulse response (FIR [35]) filter of length $N+1$.

$$\hat{s}_p = \sum_{m=p-N}^{p} h_{p-m} x_m = \sum_{j=0}^{N} h_j x_{p-j}. \tag{16}$$

The coefficients h_j need to be calculated such that the MMSE is achieved.

In order to achieve this, let us first determine the optimal condition equation (i.e. the expanded error equation).

$$\epsilon = E\left\{ \left(\sum_{k=-\infty}^{+\infty} h[k]x[n-k] - s[k] \right)^2 \right\}. \tag{17}$$

The value that minimizes ϵ can the be obtained by setting $\frac{\partial \epsilon}{\partial h[m]} = 0$ for all values of m except when $h[m] = 0$.

$$\frac{\partial \epsilon}{\partial h[m]} = E\left[\left(2\sum_k h[k]x[n-k] - s[k] \right) s[n-m] \right] = 0. \tag{18}$$

Denoting $2\sum_k h[k]x[n-k] - s[k] = e$, the above equation indicates that

$$R_{es}[m] = E[e[n]s[n-m]] = 0 \quad \forall\ m. \tag{19}$$

Thus, the error is orthogonal or uncorrelated to all data used to form the optimal estimate. It may be noted here that

$$\begin{aligned} R_{es}[m] &= E\{[e[n]s[n-m]]\} \\ &= E\{[(\hat{x}[n] - x[n])s[n-m]]\} \\ &= R_{\hat{x}s}[m] - R_{xs}[m]. \end{aligned} \tag{20}$$

In other words, the orthogonality principle can also be stated as

$$R_{\hat{x}s}[m] = R_{xs}[m]. \tag{21}$$

To find the actual values of $h[n]$, the following relation is used.

$$R_{\hat{x}s}[m] = h[m] * R_{ss}[m] = R_{xs}[m]. \tag{22}$$

An equivalent way to state this is

$$\sum_k h[k] R_{ss}[m-k] = R_{xs}[m]. \tag{23}$$

The above equation is a set if linear equations that needs to be solved for the values of $h[n]$. For a filter of length $N+1$, there are $N+1$ equations of $N+1$ values of $h[n]$. In matrix form, these equations can be written as

$$\begin{bmatrix} R_{ss}[0] & R_{ss}[1] & \dots & R_{ss}[N] \\ R_{ss}[1] & \dots & \dots & \dots \\ \dots & \dots & \dots & R_{ss}[1] \\ R_{ss}[N] & \dots & R_{ss}[1] & R_{ss}[0] \end{bmatrix} \begin{bmatrix} h_0 \\ \dots \\ \dots \\ h_N \end{bmatrix} = \begin{bmatrix} R_{xs}(0) \\ \dots \\ \dots \\ R_{xs}(N) \end{bmatrix}$$

In a compact form, h is given by

$$h = R_s^{-1} R_{xs}. \tag{24}$$

These are the Yule-Walker Eq. [36]. It is noted that $R_x \geq 0$. The matrix on the left is a Toeplitz matrix, i.e. constant along the diagonals. They can be solved by Levinson-Durbin [37] methods that are standard applications in software packages like the MATLAB [38].

The MMSE can now be computed as follows [39]:

$$E[(\hat{s}_p - s_p)^2] = R_{ss}[0] - h^T R_{xs}. \tag{25}$$

B. How to find $\Gamma(p,k)$: Relation between *local a priori* and *local a posteriori* snr

In order to obtain the mathematical form of the estimate of $\Gamma(p,k)$, we introduce the relation between the *a priori* and *a posteriori* snr by following an approach developed in [40].

Assuming the model given in Eq. (3), the amplitude of the noisy signal is given by,

$$\begin{aligned} |X(p,k)| = (&|S(p,k)|^2 + |N(p,k)|^2 \\ &+ 2|S(p,k)||N(p,k)|\cos\beta(p,k))^{\frac{1}{2}} \end{aligned} \tag{26}$$

where $\beta(p,k)$ is the phase angle between $S(p,k)$ and $N(p,k)$. Assuming that we now have some knowledge of the signal and noise from Eqs. (13) and (15), let us define a *local a priori* and *a poteriori* snr as follows.

$$snr^{\text{local}}_{\text{post}}(p,k) = \frac{|X(p,k)|^2}{|N(p,k)|^2} \tag{27}$$

and

$$snr^{\text{local}}_{\text{priori}}(p,k) = \frac{|S(p,k)|^2}{|N(p,k)|^2} \tag{28}$$

Using Eq. (26) in Eq. (27), we get

$$\begin{aligned} snr^{\text{local}}_{\text{post}}(p,k) = 1 &+ snr^{\text{local}}_{\text{priori}}(p,k) \\ &+ 2\sqrt{snr^{\text{local}}_{\text{priori}}(p,k)} \times \cos\beta(p,k) \end{aligned} \tag{29}$$

For Wiener filter, $snr_{\text{post}}(p,k)$ is assumed to be equal to $1 + snr_{\text{priori}}(p,k)$. This implies that the phase difference is constant, or, $\beta(p,k) = \pi/2$ or, the signal and the noise add in quadrature. This is also already seen in Sec. II.

IV. INFORMATION FROM THE PREVIOUS TIME FRAME: THE DECISION DIRECTED APPROACH

A. Principle

One of the most commonly used methods to obtain an estimator is known as the "decision directed" (DD) [16,17] approach. The DD estimator combines the estimated amplitude of the previous time frame and the noisy amplitude of the current frame under analysis into one estimator of the signal spectrum. Using the noise psd, the *a priori* and *a posteriori* snrs are computed as follows.

$$\widehat{snr}_{\text{post}}(p,k) = \frac{|X(p,k)|^2}{P_{NN}(p,k)} \tag{30}$$

and

$$\widehat{snr}^{DD}_{\text{priori}}(p,k) = \epsilon \frac{|\tilde{S}(p-1,k)|^2}{P_{NN}(p,k)} + (1-\epsilon)P[\widehat{snr}_{\text{post}}(p,k)-1] \tag{31}$$

where $\tilde{S}(p-1,k)$ stands for estimated signal spectrum at the previous frame and $P[\widehat{snr}_{\text{post}}(p,k)-1]$ is the half wave rectification (HWR). The HWR in this case implies that the maximum relative to zero, is taken into account.$P[.]$ or the HWR has the following properties.

$$\begin{aligned} P[x'] &= x' \quad \text{if } x' \geq 0 \\ P[x'] &= 0 \quad \text{otherwise.} \end{aligned} \tag{32}$$

This is made to ensure that the result is not negative. ϵ is chosen to be 0.98. The above estimate is the DD estimate [17]. The estimator is obtained by combining Eqs. (14) and (15). The main idea here is that the signal amplitude is estimated from the $(p-1)$th frame instead of the amplitude itself in the pth frame. It is so named because $\widehat{snr}^{DD}_{\text{priori}}(p,k)$ is updated on the basis of the previous signal amplitude estimate.

With the spectral gain being chosen as the Wiener filter [34], we have

$$\Gamma_{DD}(p,k) = \frac{\widehat{snr}^{DD}_{\text{priori}}(p,k)}{1+\widehat{snr}^{DD}_{\text{priori}}(p,k)} \tag{33}$$

Derivation of Eq. (32) is given in detail in [17].

1. Consequences

Two observations are important here: (i) when the instantaneous snr is $\gg 0$, $snr_{\text{priori}}(p,k)$ corresponds to a frame delayed version of the instantaneous snr; (ii) when the instantaneous snr is <0 or $=0$, $snr_{\text{priori}}(p,k)$ corresponds to a highly smoothed and delayed version of instantaneous snr. These two effects are observed from Eq. (11). This means that the variance of the *a priori* snr is reduced compared to the instantaneous snr. The direct effect of this phenomenon is the reduction of underlying noise to effectively enhance the signal [16].

However, it may be noted that the delay inherent to the DD algorithm can be a drawback especially in the beginning and end of the signal. Furthermore, this delay introduces a bias in gain estimation which limits noise reduction performance.

To explain this effect more, let us consider that a signal appears in frame p. Thus, *a priori* snr is zero in frame $(p-1)$. In the current frame, we have

$$\widehat{snr}^{DD}_{\text{priori}}(p,k) = (1-\epsilon)P[\widehat{snr}_{\text{post}}(p,k)-1)]. \tag{34}$$

Thus, from Eq. (10), the estimated *a priori* snr is the attenuated version of the instantaneous snr, the attenuation factor being $(1-\epsilon)$. If the phase factor $\beta(p,k)$ in Eq. (31) is $\frac{\pi}{2}$,

$$\widehat{snr}^{\text{local}}_{\text{priori}}(p,k) = [\widehat{snr}_{\text{post}}(p,k)-1] = \widehat{snr}^{\text{local}}_{ins}(p,k). \tag{35}$$

In the case that the signal ends in a frame, the *a priori* snr may be overestimated. In this case, the second term in Eq. (31) is zero, leading the estimate to have a nonzero value determined by the first term. However, a null value is desired. Thus the signal spectrum may be overestimated.

V. OVERCOMING THE OVERESTIMATION PROBLEM: TWO STEP NOISE REDUCTION TECHNIQUE USING INFORMATION FROM A LATER FRAME

In order to avoid some of the problems faced in the estimation of the *a priori* snr, a two step noise reduction (TSNR) technique has been developed. The DD algorithm introduces a frame delay when ϵ is ~ 1. As a result of this, the spectral gain matches the values in the pth and the $(p-1)$th frame. We now adopt a two step approach by applying the DD algorithm to the $(p+1)$th frame too. In this approach, we first calculate spectral gain as given by Eq. (33). In the next step, this gain is used to calculate the *a priori* snr in the $(p+1)$th frame. The gain factor is given by

$$\widehat{snr}^{\text{TSNR}}_{\text{priori}}(p,k) = \widehat{snr}^{DD}_{\text{priori}}(p+1,k). \tag{36}$$

Hence,

$$\widehat{snr}^{\text{TSNR}}_{\text{priori}}(p,k) = \frac{|\Gamma_{DD}(p,k)X(p,k)|^2}{P_{NN}(p,k)}. \tag{37}$$

It is possible to write this step by putting the weight factor in Eq. (31) equal to 1. Finally, the spectral gain is calculated as follows.

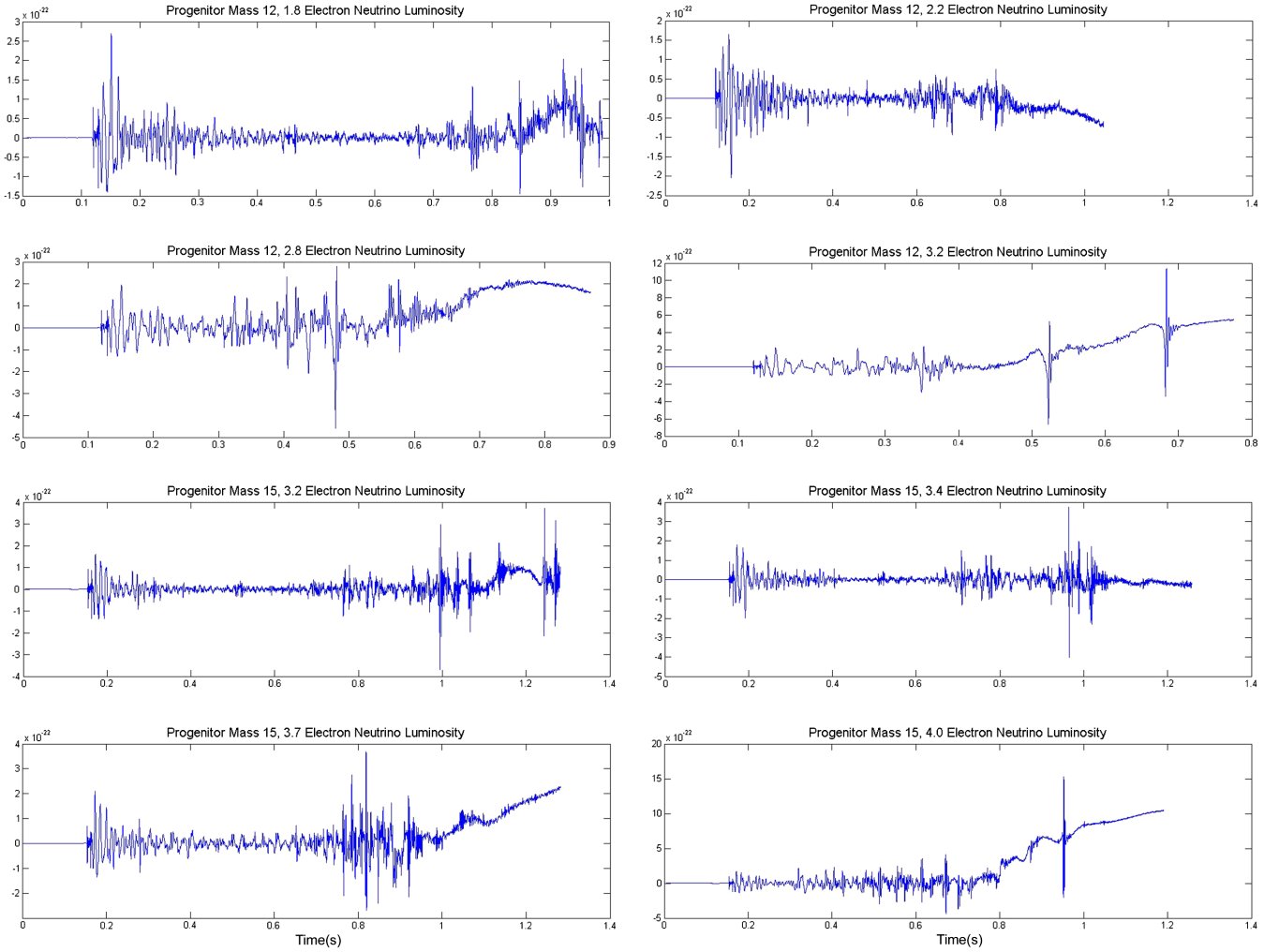

FIG. 1. The figure shows 8 supernovae waveforms used in the study from Murphy *et al.* 2009 catalog [9] with progenitor masses 12 and 15.

$$\Gamma_{\mathrm{TSNR}}(p,k) = \frac{\widehat{snr}^{\mathrm{TSNR}}_{\mathrm{priori}}(p,k)}{1+\widehat{snr}^{\mathrm{TSNR}}_{\mathrm{priori}}(p,k)} \tag{38}$$

and hence the enhanced signal estimate is

$$\hat{S}(p,k) = \Gamma_{\mathrm{TSNR}}(p,k)X(p,k). \tag{39}$$

As before, we have taken the chosen spectral gain to be the Wiener filter [34].

To summarize, the TSNR algorithm improves the noise reduction performance since the gain matches to the current frame whatever the snr.

To understand the improvement more clearly, the following is observed: (i) when the instantaneous snr is $\gg 0$, $snr^{\mathrm{TSNR}}_{\mathrm{priori}}(p,k)$ corresponds to the instantaneous snr without any delay as was found in the DD approach. Further, as the $\widehat{snr}_{ins}(p,k)$ increases or decreases (corresponding to onset and offset of the signal), the response of the $snr^{\mathrm{TSNR}}_{\mathrm{priori}}(p,k)$ is also instantaneous, unlike the DD estimator; (ii) when the instantaneous snr is < 0 or $= 0$, $snr^{\mathrm{TSNR}}_{\mathrm{priori}}(p,k)$ is reduced more compared to the DD estimator.

A. Theoretical justification of the TSNR

If no signal is present in the $(p-1)$th frame,

$$\hat{S}(p-1,k) = 0. \tag{40}$$

At the pth frame, the DD approach gives the estimation for *a priori* snr as

$$\widehat{snr}^{DD}_{\mathrm{priori}}(p,k) = (1-\epsilon)P(\widehat{snr}_{\mathrm{post}}(p,k)-1). \tag{41}$$

When refining the *a priori* snr in the TSNR technique, according to Eq. (31),

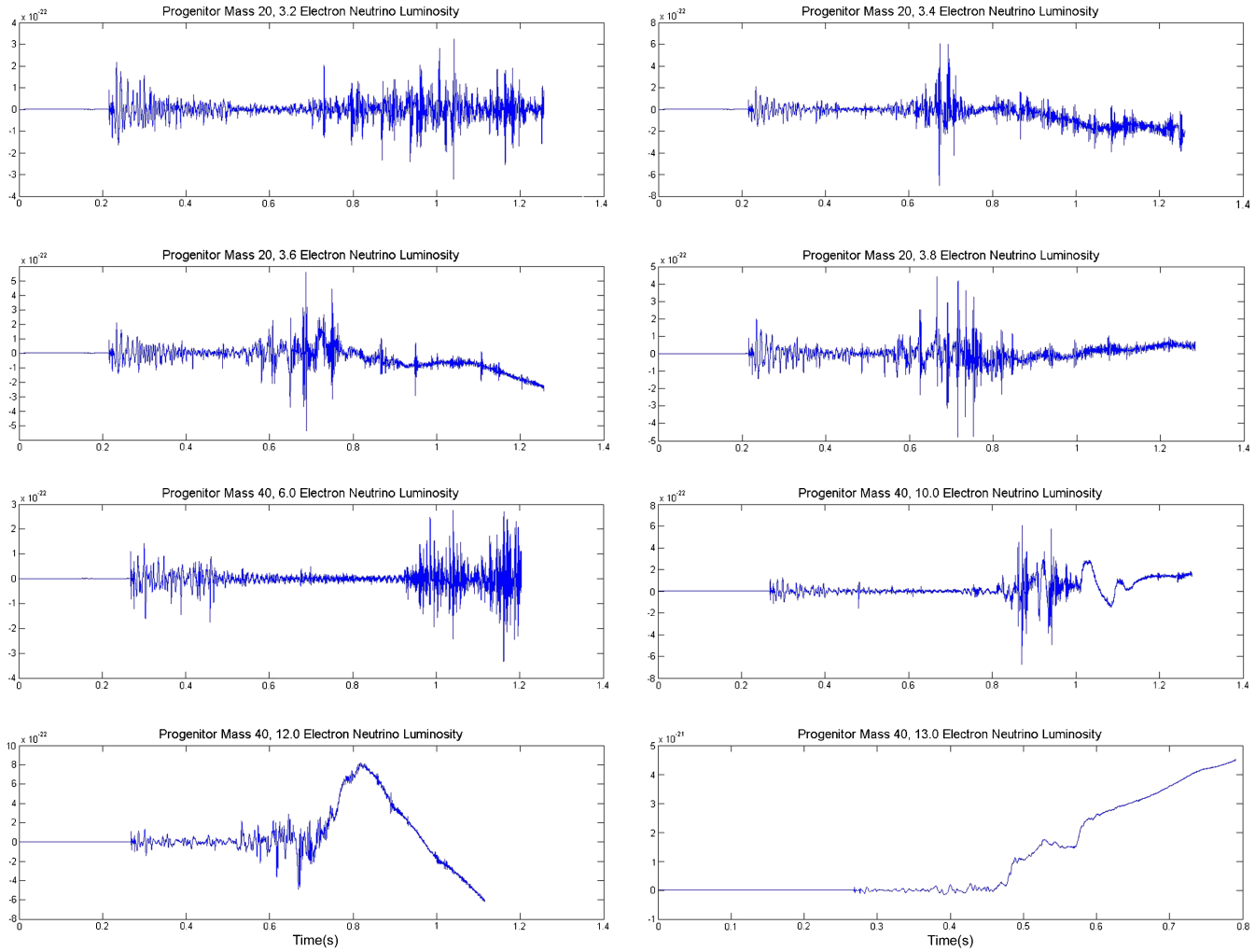

FIG. 2. The figure shows 8 supernovae waveforms used in the study from Murphy *et al.* 2009 catalog [9] with progenitor masses 20 and 40.

$$\widehat{snr}^{\mathrm{TSNR}}_{\mathrm{priori}}(p,k) = \left[\frac{(1-\epsilon)P(s\hat{n}r_{\mathrm{post}}(p,k)-1)}{1+(1-\epsilon)P(s\hat{n}r_{\mathrm{post}}(p,k)-1)}\right]^2 \times snr_{\mathrm{post}}(p,k). \tag{42}$$

By comparing Eqs. (41) and (42) to search for the intersection of the curves defined by these equations, we find that

$$\widehat{snr}_{\mathrm{post}}(p,k) > \frac{1}{2\epsilon}\left[1+2\epsilon+\sqrt{\frac{1+3\epsilon}{1-\epsilon}}\right] \tag{43}$$

It is evident from the above equation that the TSNR method delivers a greater signal power than the DD algorithm. Consequently, if a signal component appears abruptly at frame p, thus increasing the *a posteriori* snr, the estimated *a priori* snr tends to the *a posteriori* snr suppressing the bias introduced by the DD approach. This bias decreases when the *a posteriori* snr increases. However, if signal is absent at frame p too, keeping the *a posteriori* snr to a low level, the estimated *a priori* snr becomes lower than for the DD approach further limiting the noise.

Looking at the other extreme case, where *a priori* snr is higher in $(p-1)^{th}$ frame than in the p^{th} frame (i.e. the signal decays rapidly), the following approximation can be done.

$$\widehat{snr}^{DD}_{\mathrm{priori}}(p,k) \sim \epsilon\widehat{snr}_{ins}(p-1,k). \tag{44}$$

The spectral gain is then approximated as follows.

$$\Gamma_{DD}(p,k) = \frac{\epsilon\widehat{snr}_{ins}(p-1,k)}{1+\epsilon\widehat{snr}_{ins}(p-1,k)}. \tag{45}$$

Moreover, it is reasonable to assume that $\widehat{snr}_{ins}(p-1,k)$ 1 and is much greater than 1 and $\epsilon \sim 1$, Eq. (39) becomes

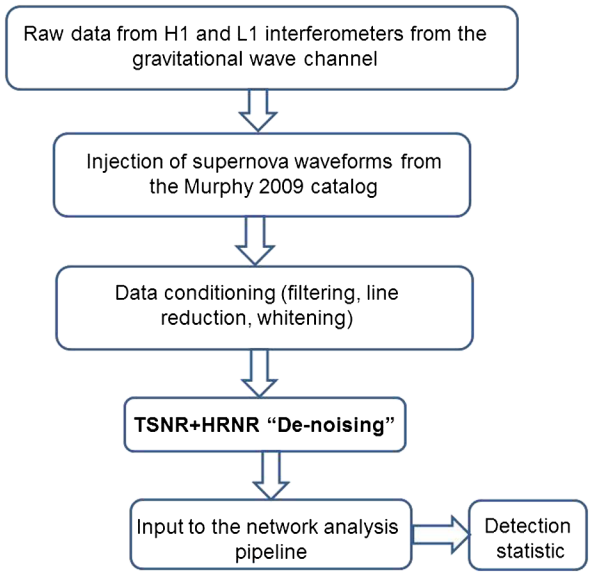

FIG. 3. The analysis pipeline starts with obtaining the raw data from three LIGO detectors (H1: Hanford 4k and L1: Livingstion 4k.) Supervovae signals are added to the data stream. The prepared data streams are now subjected to the data conditioning step where data are bandpassed between 50 Hz and 2048 Hz and all narrowband noise in this range is suppressed. The conditioned data now passes through the TSNR and HRNR module. The output from this module is supplied as the input to the network analysis pipeline. The network analysis pipeline yields the detection statistics in accordance with Eqs. (58) and (59).

$$\Gamma_{DD}(p,k) \sim 1. \tag{46}$$

Inducting this approximation in (31) leads to

$$\begin{aligned} \widehat{snr}^{\mathrm{TSNR}}_{\mathrm{priori}}(p,k) &\sim \widehat{snr}_{\mathrm{post}}(p,k), \\ &\sim \widehat{snr}_{ins}(p,k). \end{aligned} \tag{47}$$

The TSNR method leads to suppression of *a priori* snr overestimation.

VI. HARMONIC REGENERATION NOISE REDUCTION

The output signal from the previous step may still suffer some distortion due to estimation errors that may be present. It is very difficult to obtain a 100% reliable spectral estimate and hence some errors are expected to remain. Most of the distortion happend due to loss of some harmonics. The harmonic regeneration noise reduction (HRNR) consists of applying a nonlinear function to the time signal enhanced in the process described in the previous section. The restored signal is given by

$$s_{\mathrm{rectified}}(t) = \Phi(\tilde{s}(t)), \tag{48}$$

where Φ is the nonlinear function. The maximum value relative to zero (i.e. HWR) has been used in this case.

It is important to note that the $S_{\mathrm{rectified}}(t)$ are created at the same positions as the original signal, thus *no distortions are produced*. Moreover, it contains a useful information that leads to a further refinement in the *a priori* snr estimate as follows.

$$\begin{aligned} \widehat{snr}^{\mathrm{HRNR}}_{\mathrm{priori}}(p,k) = \frac{1}{P_{NN}(p,k)} &\times (\Delta(p,k)|\tilde{s}(p,k)|^2 \\ &+ (1-\Delta(p,k))|s_{\mathrm{rectified}}(p,k)|^2). \end{aligned} \tag{49}$$

The $\Delta(p,k)$ is a mixing parameter.

$$0 \le \Delta(p,k) \le 1. \tag{50}$$

Mixing is important at this stage because the nonlinear function Φ is able to restore the harmonics lost due to spectral estimation error. Δ should meet the following conditions: When $\tilde{S}(p,k)$ provided by the TSNR method is reliable, Δ is equal to 1; if the estimate is not a reliable one, $\Delta(p,k) = 0$. A standard value, e.g. 0.5, can also be used in some cases. We will use

$$\Delta(p,k) = \Gamma_{\mathrm{TSNR}}(p,k), \tag{51}$$

to meet the required conditions.

The refined *a priori* snr from Eq. (43) is now used to calculate the new spectral gain *with preservation of all features of the original signal*. As before, we have chosen the spectral gain to be the Wiener filter. Thus,

$$\Gamma_{\mathrm{HRNR}}(p,k) = \frac{\widehat{snr}^{\mathrm{HRNR}}_{\mathrm{priori}}(p,k)}{1+\widehat{snr}^{\mathrm{HRNR}}_{\mathrm{priori}}(p,k)}. \tag{52}$$

At the final stage, the desired signal spectrum is given by,

$$\tilde{\mathbf{S}}(p,k) = \Gamma_{\mathrm{HRNR}}(p,k)X(p,k) \tag{53}$$

This method is illustrated in detail in the 2006 study by Plapous *et al.* [14].

A. Theoretical explanation of HRNR

As stated in the previous section, we choose the nonlinear function Φ as follows.

$$s_{\mathrm{rectified}}(t) = Max[\hat{s}(t),0] = \hat{s}(t) \times \rho(\hat{s}(t)), \tag{54}$$

where ρ is defined as

$$\begin{aligned} \rho(g) &= 1 \quad \text{if } g > 0 \\ \rho(g) &= 0 \quad \text{if } g < 0. \end{aligned} \tag{55}$$

In other words, we have chosen the HWR. $\rho(g)$ defines an elementary repetitive waveform. It is reasonable to assume that, over a short time period, the signal is quasistationary.

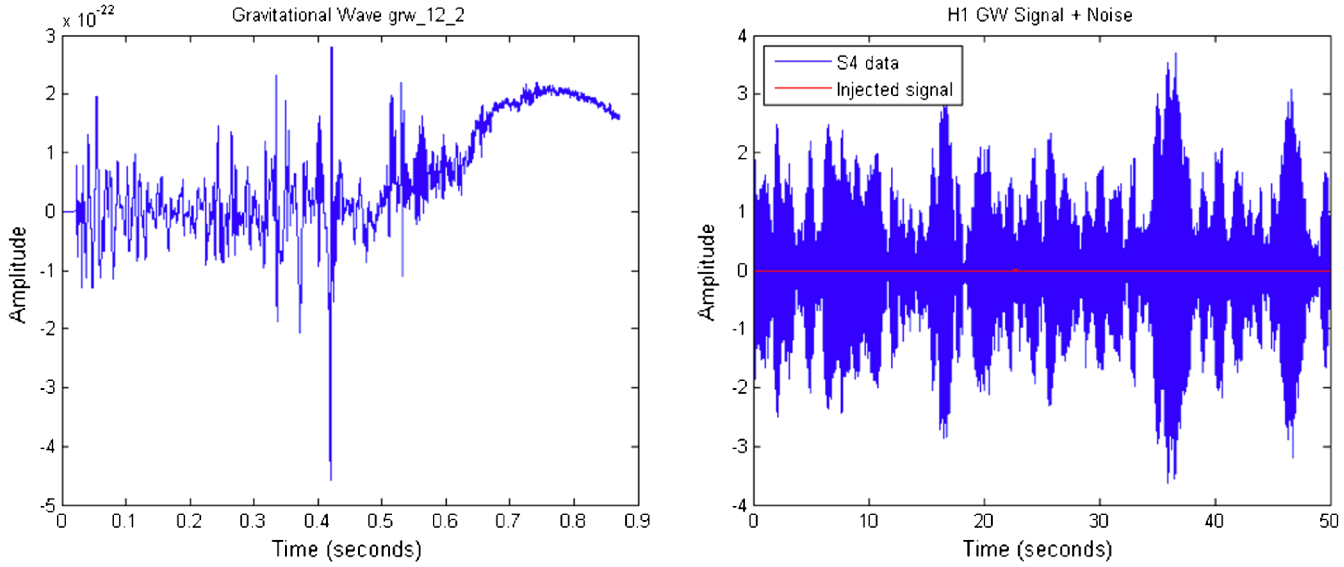

FIG. 4. The waveform (grw_12_2, left panel) is injected into the data stream (right panel) with a scale factor of 30. The x-axis represents time in seconds and the y-axis is the amplitude.

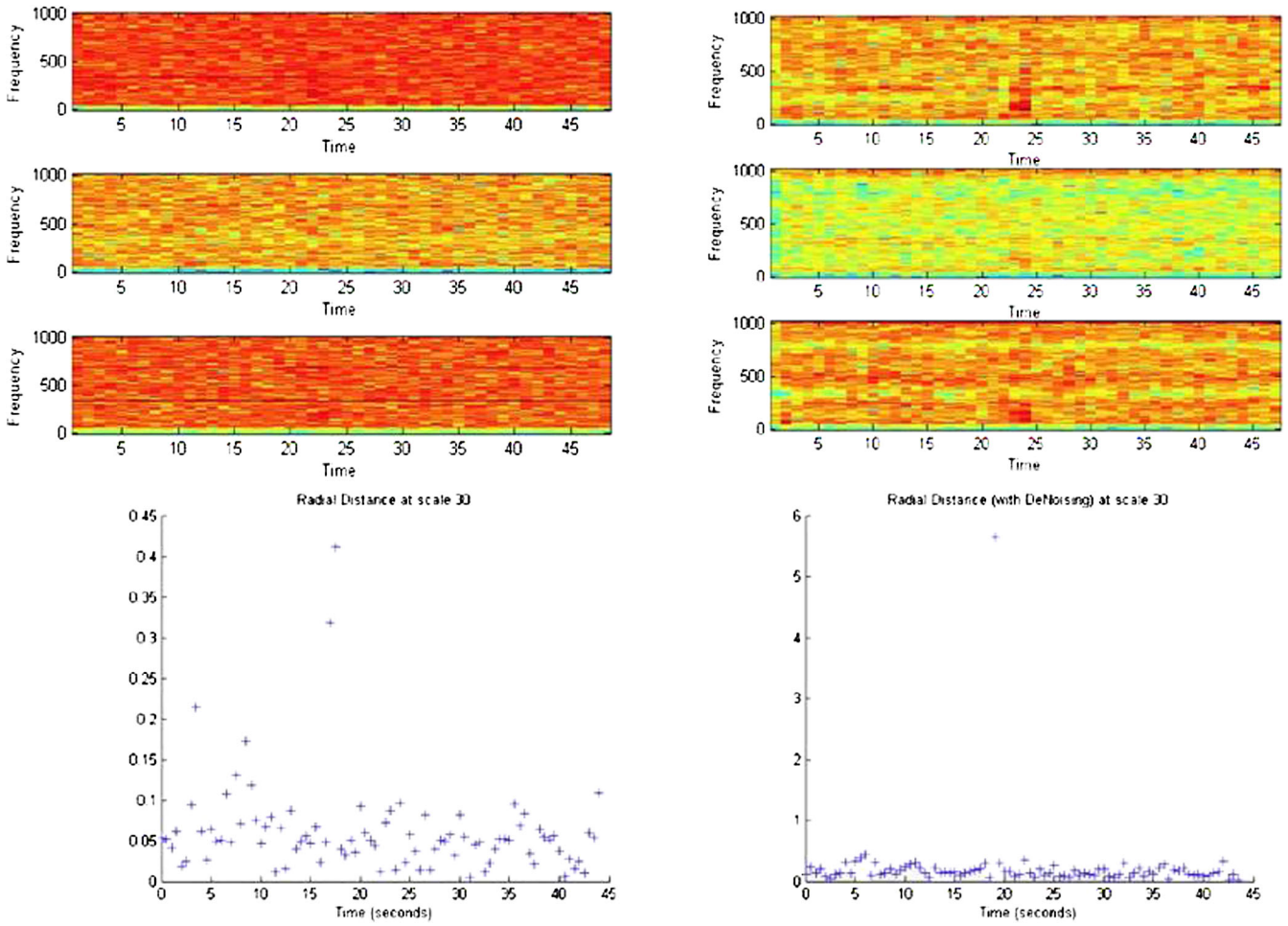

FIG. 5. The figure shows the spectrograms of the signal (grw_12_2) + noise after being conditioned without the TSNR + HRNR denoising effect (top left panel) and the same with the inclusion of the TSNR + HRNR denoising (top right panel.) The x-axis represents time in seconds and the y-axis represents frequency in Hz. The bottom row of figures shows the radial statistics (as given in equation [17]) for the analysis performed without the proposed denoising (left panel) and with the TSNR + HRNR denoising (right panel.) The x-axis represents time in seconds and the y-axis represents the radial distance.

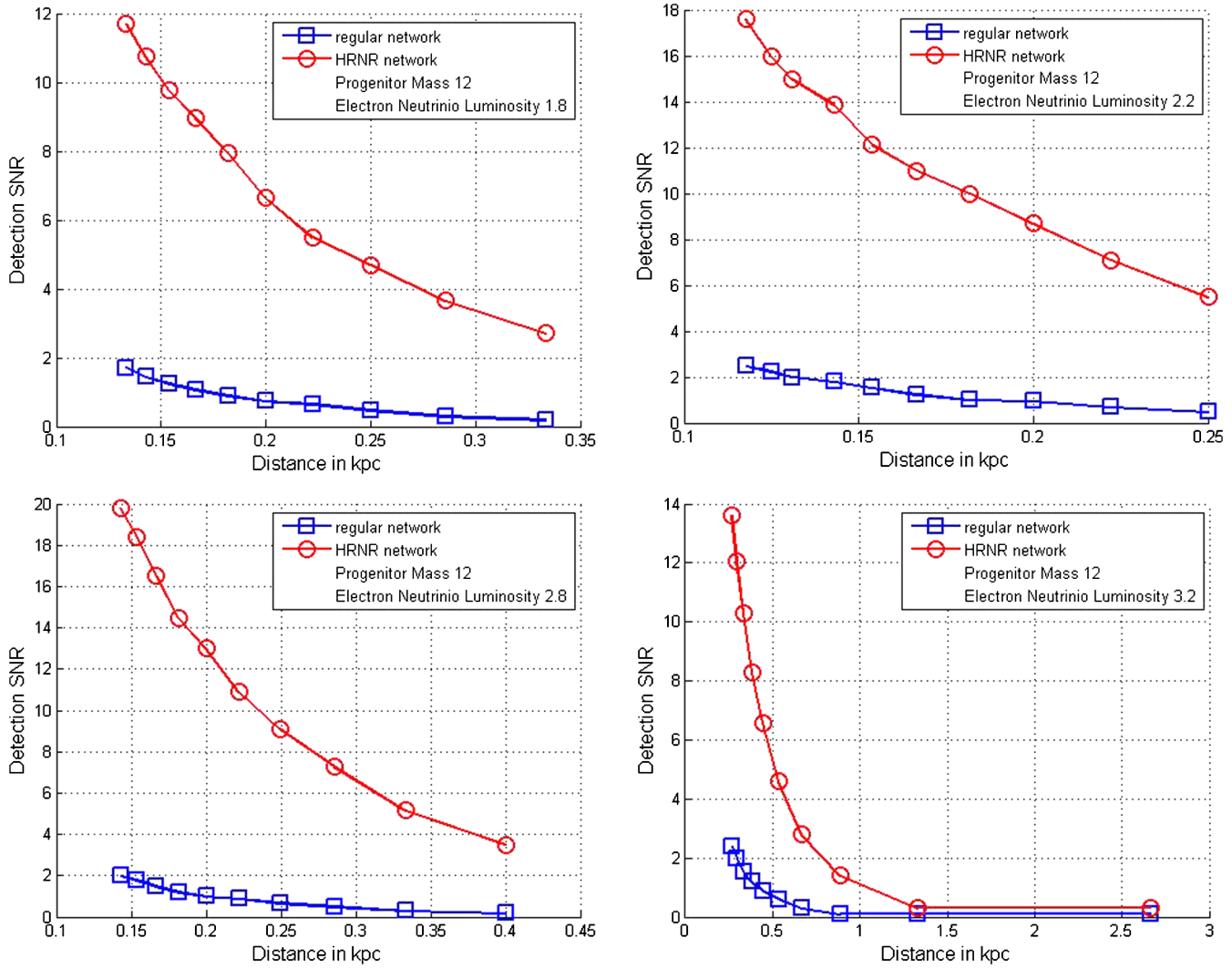

FIG. 6. The figure shows the radial statistics as a function of distance for four waveforms from the catalog. The x-axis represents the distance in kpc. The y-axis represents the detection snr defined from Eq. (59). The detection snr is equal to the average value of the radial distance $R_{\rm rad}$ subtracted from the maximum value of the same that corresponds to the event detected. The lower curve (in blue) is the operating characteristic for the original pipeline without the implementation of the proposed TSNR + HRNR denoising module. The upper curve (in red) represents the same with the incorporation of the TSNR + HRNR denoising.

The fourier transform (FT) of $\rho(g)$ is given by,

$$\tilde{\rho}(\hat{s}(t)) = \frac{1}{T}\sum_{n=-\infty}^{\infty} Q\left(\frac{n}{T}\right)\delta\left(\nu - \frac{n}{T}\right), \tag{56}$$

where δ is the Dirac delta function and ν denotes the frequency. $Q(\frac{n}{T})$ is the FT of the underlying elementary waveform at discrete frequency $\frac{n}{T}$. Using [56], the FT of $s_{\rm rectified}(t)$ is given by,

$$\tilde{S}_{\rm rectified}(t) = FT(\hat{s}(t)) \times \frac{e^{-i\theta}}{T} \times \sum_{n=-\infty}^{\infty} Q\left(\frac{n}{T}\right)\delta\left(\nu - \frac{n}{T}\right). \tag{57}$$

θ is the phase angle at the origin. In summary, the spectrum of the rectified signal is the convolution between the signal enhanced by the TSNR and a harmonic comb with the same frequency as the signal. Moreover, $\tilde{\rho}(\tilde{s}(t))$ rapidly decreases as $|n|$ increases, ensuring that regeneration takes place only using information from its near neighbors.

VII. ANALYSIS

A. Data used

Sixteen supernova waveforms from the Murphy *et al.* 2009 catalog [9] have been used in presence of LIGO fourth science run (S4 [41]) data for demonstration of results from the search algorithm. The catalog describes the GW signals from neutrino driven core collapse supernovae.

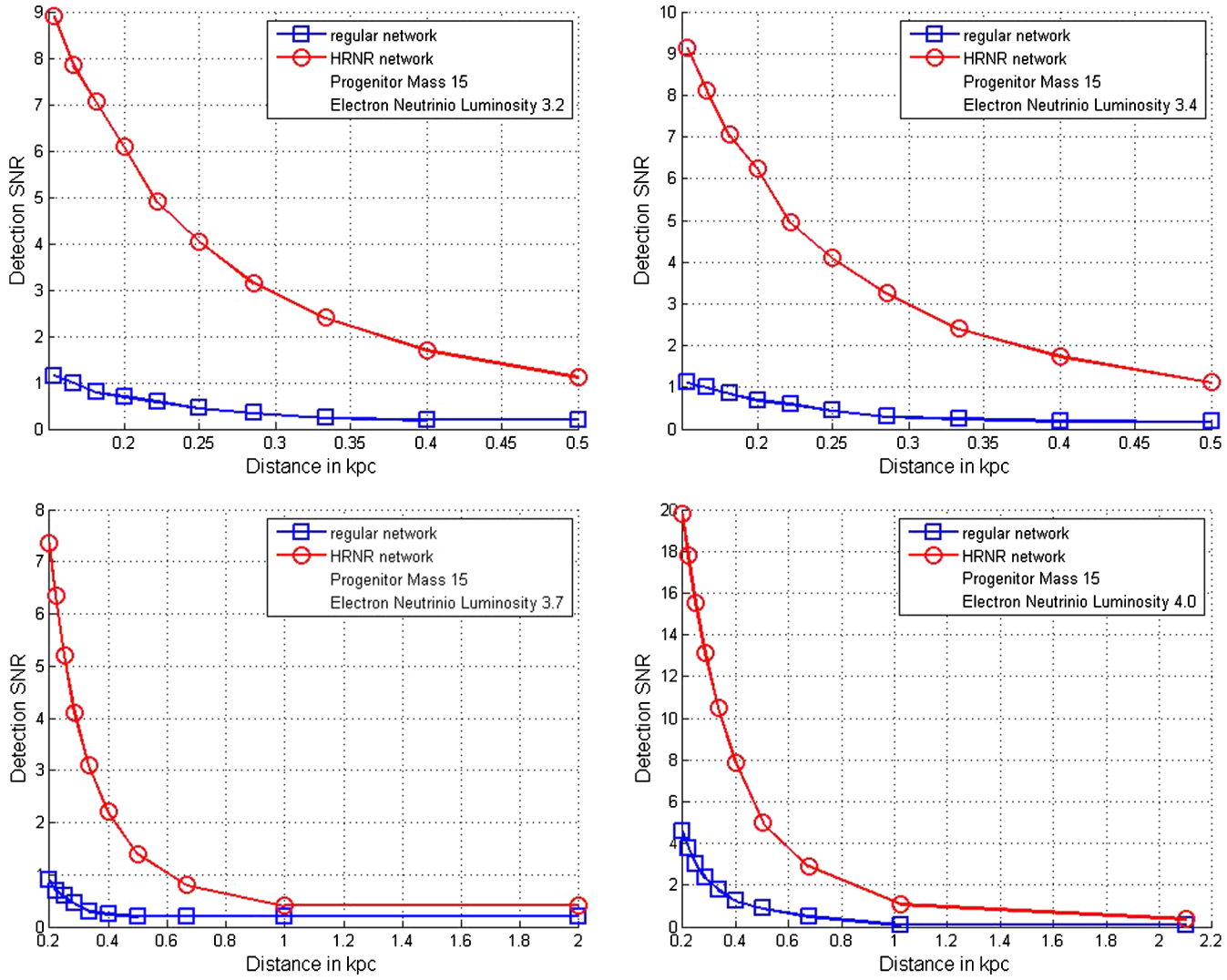

FIG. 7. The figure shows the radial statistics as a function of distance for four waveforms from the catalog. The x-axis represents the distance in kpc. The y-axis represents the detection snr defined from Eq. (59). The detection snr is equal to the average value of the radial distance $R_{\rm rad}$ subtracted from the maximum value of the same that corresponds to the event detected. The lower curve (in blue) is the operating characteristic for the original pipeline without the implementation of the proposed TSNR + HRNR denoising module. The upper curve (in red) represents the same with the incorporation of the TSNR + HRNR denoising.

The waveforms used in the study are shown in Fig. 1 and Fig. 2.

The analysis pipeline is shown in Fig. 3.

Sets of test data, each 60 seconds long, from the main GW channel (DARM_ERR) from two Hanford detectors (4 km arm-length H1 and 2 km arm-length H2) and the Livingston detector (4 km arm-length L1) are used for demonstration of results. Data streams have been injected with the signal waveforms. The signals are introduced in the data streams starting at 20 seconds after start. After this, data conditioning is applied to the data containing the signal. The data conditioning consists of the following steps. (i) Extraction of raw GW channel data with SN signals injected; let this time series be noted by T_0; (ii) Whitening T_0 [42] and dynamically removing [43,44] the narrowband noise present in T_0; The resulting time series is denoted by T_0'; (iii) Filtering T_0' with a bandwidth of 50 Hz and 2048 Hz; The resulting time series is denoted by $filt_{T_0'}$; (iv) Re-sampling $filt_{T_0'}$ to represent the appropriate band width.

The conditioned data sets are then applied to the input of the TSNR + HRNR denoising stage. The denoised output from the TSNR + HRNR module is then used as the input to a network analysis based on regularized maximum likelihood [11–13,45].

B. Detection statistics

It is known that the detector response to GW signal is a linear combination of the unknown polarization waveforms

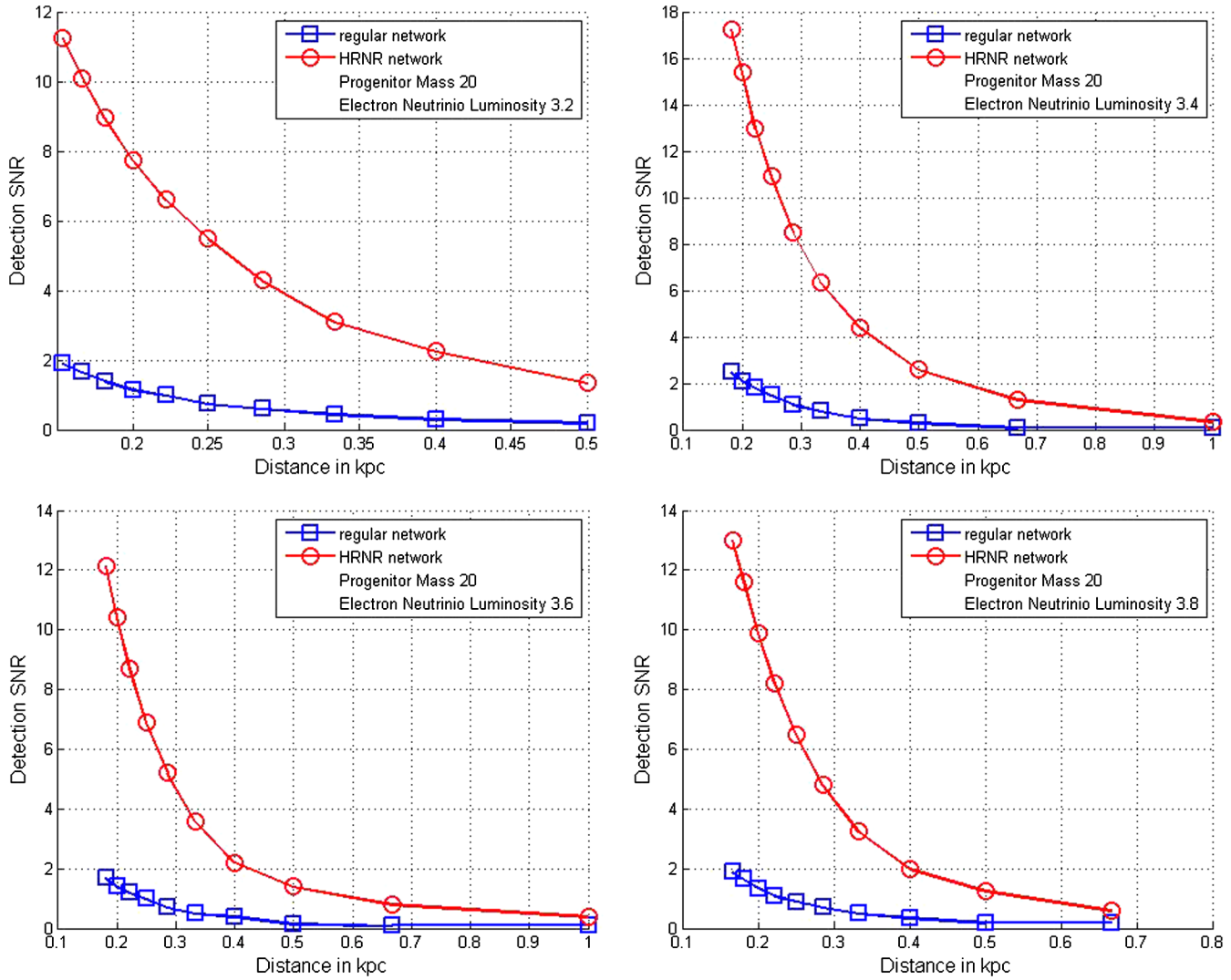

FIG. 8. The figure shows the radial statistics as a function of distance for four waveforms from the catalog. The x-axis represents the distance in kpc. The y-axis represents the detection snr defined from Eq. (59). The detection snr is equal to the average value of the radial distance $R_{\rm rad}$ subtracted from the maximum value of the same that corresponds to the event detected. The lower curve (in blue) is the operating characteristic for the original pipeline without the implementation of the proposed TSNR + HRNR denoising module. The upper curve (in red) represents the same with the incorporation of the TSNR + HRNR denoising.

$h_+(t)$ and $h_\times(t)$ arriving from a direction with polar angle θ_0 and azimuthal angle ϕ_0 in an earth-centered, ecliptic reference frame [45].

The network analysis performed is based on using a regulator (Tikhonov regularization [12]) to address the ill-posed problem of a network of gravitational wave detectors as first shown in [11,46]. The output of the network algorithm for a given sky location θ_0 and azimuthal angle ϕ_0, is the value of the likelihood of the data maximized over all possible $h_+(t)$ and $h_\times(t)$ waveforms. A skymap [11,12,45] is said to be constructed with the maximum likelihood values obtained as a function of θ_0 and azimuthal angle ϕ_0. The detection statistic is constructed from the skymap as follows.

$$R_{\rm rad} = \left[\left(\frac{\max_{\theta_0,\phi_0}\mathbf{S}(\theta_0,\phi_0)}{\max_{\theta_0,\phi_0}\mathbf{S}_0(\theta_0,\phi_0)} - 1\right)^2 + \left(R_{mm} \times \frac{\min_{\theta_0,\phi_0}\mathbf{S}_0(\theta_0,\phi_0)}{\max_{\theta_0,\phi_0}\mathbf{S}_0(\theta_0,\phi_0)} - 1\right)^2\right]^{\frac{1}{2}}, \quad (58)$$

where R_{mm} is given by

$$R_{mm} = \frac{\max_{\theta_0,\phi_0}\mathbf{S}(\theta_0,\phi_0)}{\min_{\theta_0,\phi_0}\mathbf{S}(\theta_0,\phi_0)}, \quad (59)$$

and $\mathbf{S}_0$ is the expectation value of $\mathbf{S}$ when no signal is present in the data. $R_{\rm rad}$ is known as the radial statistics. It denotes the radial distance of the observed values in the

$(R_{mm}, \max_{\theta_0,\phi_0} \mathbf{S}(\theta_0, \phi_0)$ plane from the mean location in absence of the signal. The larger the radial distance, the higher is the detection probability.

VIII. RESULTS

Figures 4 and 5 show the analysis results for one of the catalog waveforms (grw_12_2; progenitor mass 12, electron neutrino luminosity 2.2) injected into the data stream with a scale factor of 30, i.e. the original signal was multiplied by a factor of 30. Figure 4 shows the signal injected into the detector noise. For reference, a scale factor of 30 corresponds to the snr threshold below which the signal is not discerned in the network analysis radial distance statistics without the application of the TSNR + HRNR denoising module. Figure 5 top row shows the spectrograms of the signal + noise data after being conditioned without the TSNR + HRNR denoising effect (left panel) and the same with the inclusion of the TSNR + HRNR denoising (right panel.) It is clear even visually that the TSNR + HRNR denoising effectively has enhanced the snr of the embedded signal. The bottom row shows the radial statistics (as given in equation [59]) for the analysis performed without the proposed denoising (left panel) and with the TSNR + HRNR denoising (right panel.) In the first case, the max value of $R_{\rm rad}$ is around 0.4, while in the second case, it is about 5.5, an improvement of a factor of 14. It may be noted that the noise scatter is much less in the second case than the first one. This significant reduction of the range of variability of the detection statistics for the noise events with respect to the injected signals is

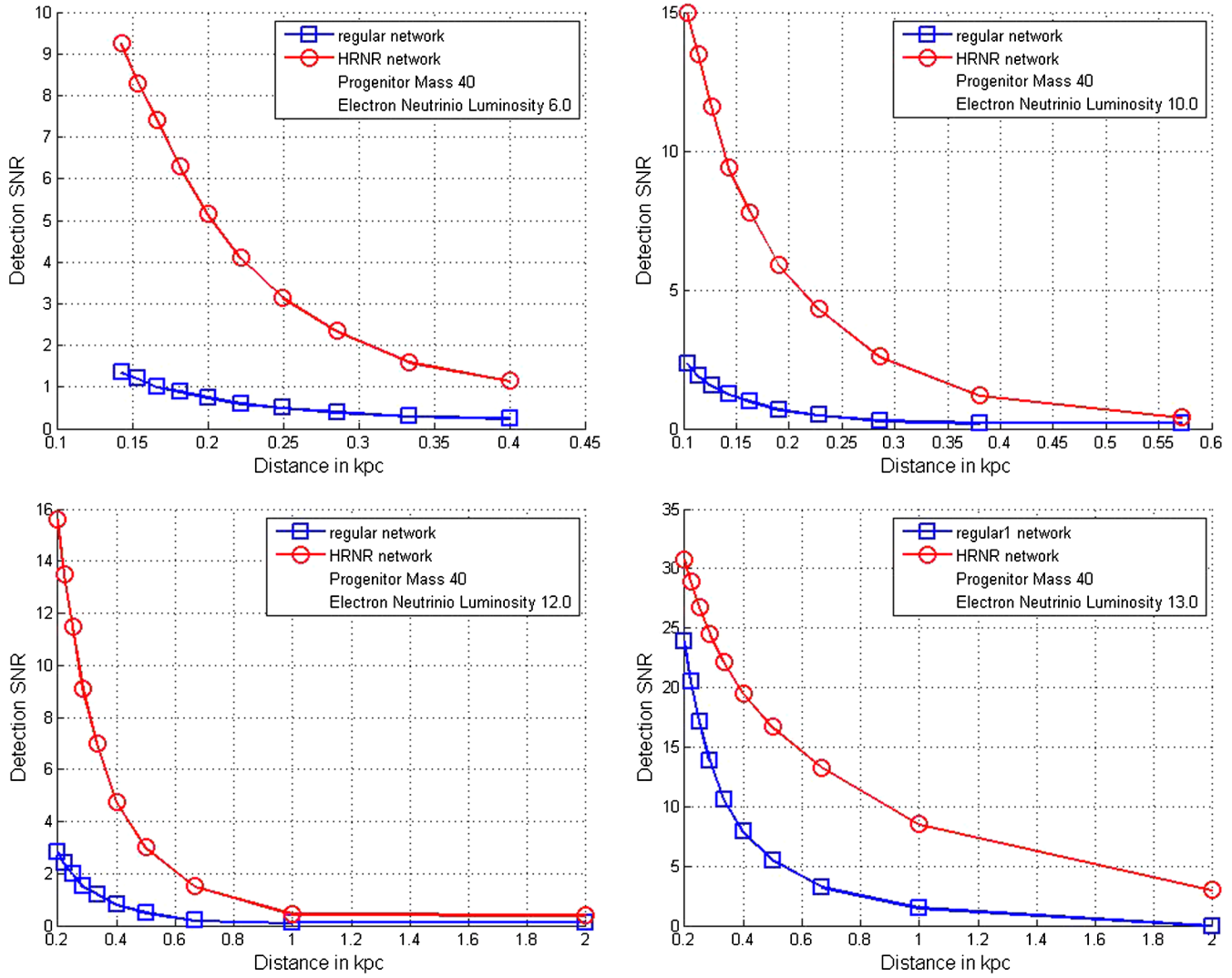

FIG. 9. The figure shows the radial statistics as a function of distance for four waveforms from the catalog. The x-axis represents the distance in kpc. The y-axis represents the detection snr defined from Eq. (59). The detection snr is equal to the average value of the radial distance $R_{\rm rad}$ subtracted from the maximum value of the same that corresponds to the event detected. The lower curve (in blue) is the operating characteristic for the original pipeline without the implementation of the proposed TSNR + HRNR denoising module. The upper curve (in red) represents the same with the incorporation of the TSNR + HRNR denoising.

important. In the left panel, a reduction of the detection statistics by 30% makes the GW less significant than a noise event. In the right panel, even a reduction by a factor of 5 leaves the GW as the loudest event. This is important because recent GW detection schemes in LIGO strongly rely on the loudest event in the data.

Figures 6–9 show the core of analysis results. These plots correspond to the 16 Murphys waveforms that have been analyzed. The progenitor masses varied from 12 to 40 with various luminosity values between 1.8 and 13.0. The x-axis represents distance in kpc and the y-axis reprsents the detection snr defined from Eq. (59). The detection snr is equal to the average value of the radial distance $R_{\rm rad}$ subtracted from the maximum value of the same that corresponds to the event detected. The lower curve (in blue) is the operating characteristic for the original pipeline without the implementation of the proposed TSNR + HRNR denoising module. The upper curve (in red) represents the same with the incorporation of the TSNR + HRNR denoising. As can be seen, for all the 16 waveforms, the detection snr is higher across the distances for the combined HRNR + TSNR pipeline. It must be noted that at this stage, the actual values of the distances are not of any physical significance because we have used data from S4 just for demonstration of the method's efficiency.

A companion paper has been prepared with results from more recent science runs. More extensive testing has been performed with sine-Gaussian, Murphy, long-bar, rotating core collapse (Dimmermeier [47]) waveforms by integrating this method to existing coherent wave burst (cWB)-based [13,48] supernova search pipeline. More supernova signals will be incorporated in the study. Receiver operating characteristics (ROC) will be generated for a comparative performance analysis. It will indeed be interesting to note if the improvement in detection statistics noted in this study also remains persistent in the future studies as the advanced LIGO [7] comes into operation.

IX. CONCLUSION

The result shows improvement in detection statistics (as defined and described in detail in Sec. VI B) by a factor of up to 10 even for very weak snr. The improvement in the detection statistics grows steadily with increasing signal strengths. HRNR works robustly even with non-stationary, non-gaussian noise. A major advantage of the proposed method is that it is a stand-alone MATLAB [38] code module that can be easily plugged in to existing search pipelines without having to make alterations. HRNR contains adjustable parameters that can in principle improve the results even more.

It is worth mentioning here the work of Oppermann *et al.* [49]. In a study to reconstruct Gaussian signals from linear measurements with Gaussian noise with uncertainties in the signal covariance, the authors have formulated and applied a *critical filter* [50] in the context of image reconstruction. The study makes a comparison of this method with that of the Wiener filter. If the correct power spectrum is known and noise is homogeneous, the reconstruction is known to be optimal. In the cases with inhomogeneous noise, the Wiener filter fails to completely clean out the noise, as is expected. However, if the noise is not estimated correctly, problems similar to that see in the case of Wiener filter applications are noticed. An amplifying effect appears in the estimated power spectrum especially where the noise is underestimated. In the present study, the effects of incorrect estimation of noise have been discussed in Sec. V. The reason a two-step approach has been adopted in this case is to avoid some of the shortcomings associated with the overestimation and underestimation of noise.

A more extensive testing with the sixth science run (S6) data has been performed with five different families of supernova waveforms by integrating this method to existing coherent waveburst supernova search pipeline. Receiver operating characteristics (ROC) and Coherent event displays (CED) are being generated for comparison. It will indeed be interesting to note if the improvement in detection statistics noted in this study also remains persistent in the future studies as the advanced LIGO [7]. With the direct observation of the first gravitational waves [51], this scenario presents an exciting possibility.

ACKNOWLEDGMENTS

This work is supported by NSF Grant No. NSF PHY 1205585 (2012). J. M. is supported by NSF Research Experience for Undergraduates grant at the University of Texas Rio Grande Valley in 2014. Use of LIGO fourth science run data is acknowledged. Many thanks to Dr. Michele Zanolin for a careful reading of the manuscript.

[1] C. D. Ott, E. Abdikamalov, E. O'Connor, C. Reisswig, R. Haas, P. Kalmus, S. Drasco, A. Burrows, and E. Schnetter, Correlated gravitational wave and neutrino signals from general-relativistic rapidly rotating iron core collapse, Phys. Rev. D **86**, 024026 (2012).

[2] C. D. Ott, C. Reisswig, E. Schnetter, E. Connor, U. Sperhake, F. Lffler, P. Diener, E. Abdikamalov, I. Hawke, and A. Burrows, Dynamics and Gravitational Wave Signature of Collapsar Formation, Phys. Rev. Lett. **106**, 161103 (2011).

[3] E. Abdikamalov, C. D. Ott, L. Rezzolla, L. Dessart, H. Dimmelmeier, A. Marek, and H.-T. Janka, Axisymmetric General relativistic simulations of the accretion-induced collapse of white dwarfs, Phys. Rev. D **81**, 044012 (2010).
[4] A. Abramovici, W. Althouse, R. Drever, Y. Gursel, S. Kawamura, F. Raab, D. Shoemaker, L. Sievers, R. Spero, K. Thorne, R. Vogt, R. Weiss, S. Whitcomb, and M. Zucker, LIGO: The Laser Interferometer Gravitational-Wave Observatory, Science **256**, 325 (1992).
[5] T. Accadia, F. Acernese, F. Antonucci *et al.*, Status and perspectives of the Virgo gravitational wave detector, J. Phys. Conf. Ser. **203**, 012074 (2010).
[6] H. Grote, K. Danzmann, K. L. Dooley, R. Schnabel, J. Slutsky, and H. Vahlbruch, First Long-Term Application of Squeezed States of Light in a Gravitational-Wave Observatory, Phys. Rev. Lett. **110**, 181101 (2013).
[7] G. M. Harry (for the LIGO Scientific Collaboration) Advanced LIGO: The next generation of gravitational wave detectors, Classical Quantum Gravity **27**, 084006 (2010).
[8] B. Muller, H.-T. Janka, and A. Marek, A new multidimensional general relativistic neutrino hydrodynamics code of core-collapse supernovae. III. Gravitational wave from supernova emission models, Astrophys. J. **766**, 43 (2013).
[9] J. W. Murphy, C. D. Ott, and A. Burrows, A model for gravitational wave emission in neutrino-driven core-collapse supernovae, Astrophys. J. **707**, 1173 (2009).
[10] K. N. Yakunin, P. Marronetti, A. Mezzacappa *et al.*, Gravitational waves from core collapse supernovae, Classical Quantum Gravity **27**, 194005 (2010).
[11] S. D Mohanty, M. Rakhmanov, S. Klimenko, and G. Mitselmakher, Penalized likelihood, Classical Quantum Gravity **23**, 4799 (2006).
[12] M. Rakhmanov, Rank deficiency of network matrix, Classical Quantum Gravity **23**, S673 (2006).
[13] S. Klimenko, S. D. Mohanty, M. Rakhmanov, and G. Mitselmakher, Constraint likelihood analysis for a network of gravitational wave detectors, Phys. Rev. D **72**, 122002 (2005).
[14] C. Plapous, C. Marro, and P. Scalart, Improved signal-to-noise ratio estimation for speech enhancement, IEEE Transactions on Audio Speech and Language Processing **14**, 2098 (2006).
[15] P. Scalart and J. V. Filho, Speech enhancement based on *a priori* signal to noise estimation, Proc. IEEE Int. Conf. Acoust., Speech, Signal Process. **2**, 629632 (1996).
[16] O. Cappe, Elimination of the musical noise phenomenon with the Ephraim and Malah noise suppressor, IEEE Trans. Speech Audio Process. **2**, 345 (1994).
[17] Y. Ephram and D. Malah, Speech enhancement using a minimum mean-square error short-time spectral amplitude estimator, IEEE Trans. Acoust., Speech, Signal Process. **32**, 1109 (1984).
[18] J. Logue, C. D. Ott *et al.*, Inferring core-collapse supernovae physics with gravitational waves, Phys. Rev. D **86**, 044023 (2012).
[19] D. S. Sivia and J. Skilling, *Data Analysis: A Bayesian Tutorial*, 2nd ed. (Oxford University Press, New York, 2006).
[20] J. Skilling, Nested Sampling, AIP Conf. Proc. **735**, 395 (2004).
[21] stellarcollapse.org.
[22] S. E. Gossan, P. Sutton, A. Stuver, M. Zanolin, K. Gill, and C. D. Ott, Observing gravitational waves from core-collapse supernovae in the advanced detector era, Phys. Rev. D **93**, 042002 (2016).
[23] P. J. Sutton, G. Jones *et al.*, X-Pipeline: an analysis package for autonomous gravitational-wave burst searches, New J. Phys. **12**, 053034 (2010).
[24] A. L. Piro and E. Pfahl, , Fragmentation of Collapsar Disks and the Production of Gravitational Waves, Astrophys. J. **658**, 1173 (2007).
[25] C. D. Ott (LIGO Scientific Collaboration), Technical Report No. LIGO-T1000553-v2: dcc.ligo.org/LIGO-T1000553/public.
[26] J. Powell, S. E. Gossan, J. Logue, and I. S. Heng, Inferring the core-collapse supernova explosion mechanism with gravitational waves, Phys. Rev. D **94**, 123012 (2016).
[27] K. Hayama, T. Kuroda, K. Kotake, and T. Takiwaki, Coherent network analysis of gravitational waves from three-dimensional core-collapse supernova models, Phys. Rev. D **92**, 122001 (2015).
[28] A. Tomotada (KAGRA collaboration), Large-scale cryogenic gravitational-wave telescope in Japan: KAGRA, J. Phys. Conf. Ser. **610**, 012016 (2015).
[29] S. Kay, *Fundamentals Of Statistical Signal Processing* (Prentice Hall, London, 2001) Vol. 1.
[30] S. Kay, *Fundamentals Of Statistical Signal Processing* (Prentice Hall, London, 2001) Vol. 2.
[31] C. Cutler and E. E. Flanagan, Gravitational waves from merging compact binaries: How accurately can one extract the binarys parameters from the inspiral wave form?, Phys. Rev. D **49**, 2658 (1994).
[32] J. S. Lim and A. V. Oppenhein, Enhancement and bandwidth compression of noisy speech, Proc. IEEE **67**, 1586 (1979).
[33] R. Martin, Noise power spectral density estimation based on optimal smoothing and minimum statistics, Proc. IEEE transactions on speech and audio, **9**, 504 (2001).
[34] N. Wiener, *Extrapolation, Interpolation, and Smoothing of Stationary Time Series* (Wiley, New York, 1949).
[35] H. L. Van Trees, *Detection, Estimation, and Modulation Theory (parts I and II)* (Wiley-Interscience, New York, 2001).
[36] W. Chen, B. D. O. Anderson, M. Deistler, and A. Filler, Solutions of Yule-Walker equations for singular AR processes, J. Time Ser. Anal. **32**, 531 (2011).
[37] G. H. Golub and C. F. Van Loan, *Matrix Computations*, 3rd ed. (Johns Hopkins University Press, Baltimore, MD, 1996), Sec. 4.7.
[38] www.mathworks.com.
[39] J. G. Proakis and M. Salehi, *Digital Communications*, 5th edition (McGraw-Hill College, New York, 2007).
[40] P. Renevey and A. Drygajlo, Detection of reliable features for speech recognition in noisy conditions using a statistical criterion, Proc. Workshop Consistent Reliable Acoust. Cues Sound Anal., Aalborg, Denmark, pp. 71–4, 2001.
[41] B. Abbott *et al.* (LIGO Scientific Collaboration), All-sky search for periodic gravitational waves in LIGO S4 data, Phys. Rev. D **77**, 022001 (2008).
[42] S. D. Mohanty, Median based line tracker (MBLT): model independent and transient preserving line removal from

interferometric data, Classical Quantum Gravity **19**, 1513 (2002).
[43] L. S. Finn and S. Mukherjee, Data conditioning for gravitational wave detectors: A Kalman filter for regressing suspension violin modes, Phys. Rev. D **63**, 062004 (2001).
[44] A. Sintes and B. F. Schutz, Removing non-stationary, non-harmonic external interference from gravitational wave interferometer data, Phys. Rev. D **60**, 062001 (1999).
[45] K. Hayama, S. D. Mohanty, M. Rakhmanov, and S. Desai, Coherent network analysis for triggered gravitational wave burst searches, Classical Quantum Gravity **24**, S681 (2007).
[46] W. R. Johnston, Masters thesis, The University of Texas at Brownsville, 2004.
[47] H. Dimmelmeier, J. A. Font, and E. Muller, Relativistic simulations of rotational core collapse II. Collapse dynamics and gravitational radiation, Astron. Astrophys. **393**, 523 (2002).
[48] S. Klimenko, I. Yakushin, A. Mercer, and G. Mitselmakher, Coherent method for detection of gravitational wave bursts, Classical Quantum Gravity **25**, 114029 (2008).
[49] N. Oppermann, G. Robbers, and T. A. Ensslin, Reconstructing signals from noisy data with unknown signal and noise covariance, Phys. Rev. E **84**, 041118 (2011).
[50] N. Oppermann, H. Junklewitz *et al.*, An improved map of the Galactic Faraday sky, Astron. Astrophys. **542**, A93 (2012).
[51] B. P. Abbott *et al.* (LIGO Scientific Collaboration), Observation of Gravitational Waves from a Binary Black Hole Merger, Phys. Rev. Lett. **116**, 061102 (2016).